The Astrophysical Journal, 805:60 (8pp), 2015 May 20 doi:10.1088/0004-637X/805/1/60

EVIDENCE FOR AN INTERSTELLAR DUST FILAMENT IN THE OUTER HELIOSHEATH

P. C. Frisch[1], B-G Andersson[2], A. Berdyugin[3], V. Piirola[3], H. O. Funsten[4], A. M. Magalhaes[5], D. B. Seriacopi[5], D. J. McComas[6,10], N. A. Schwadron[7], J. D. Slavin[8], and S. J. Wiktorowicz[9]
[1] Department of Astronomy and Astrophysics, University of Chicago, Chicago, IL 60637, USA
[2] SOFIA, USRA, CA, USA
[3] Finnish Centre for Astronomy with ESO, University of Turku, Finland
[4] Los Alamos National Laboratory, Los Alamos, NM, USA
[5] Instituto de Astronomia, Geofisica e Ciencias Atmosfericas, Universidade de Sao Paulo, Brazil
[6] Southwest Research Institute, San Antonio, TX, USA
[7] Space Science Center, University of New Hampshire, Durham, NH, USA
[8] Harvard-Smithsonian Center for Astrophysics, Cambridge, MA, USA
[9] Department of Astronomy, University of California at Santa Cruz, Santa Cruz, CA, USA
Received 2015 January 19; accepted 2015 March 14; published 2015 May 20

ABSTRACT

A recently discovered filament of polarized starlight that traces a coherent magnetic field is shown to have several properties that are consistent with an origin in the outer heliosheath of the heliosphere: (1) the magnetic field that provides the best fit to the polarization position angles is directed toward $\ell = 357.^{\circ}3$, $b = 17.^{\circ}0$ ($\pm 11.^{\circ}2$); this direction is within $6.^{\circ}7 \pm 11.^{\circ}2$ of the observed upwind direction of the flow of interstellar neutral helium gas through the heliosphere. (2) The magnetic field is ordered; the component of the variation of the polarization position angles that can be attributed to magnetic turbulence is $\pm 9.^{\circ}6$. (3) The axis of the elongated filament can be approximated by a line that defines an angle of $80^{\circ} \pm 14^{\circ}$ with the plane that is formed by the interstellar magnetic field (ISMF) vector and the vector of the inflowing neutral gas (the ***BV*** plane). We propose that this polarization feature arises from aligned interstellar dust grains in the outer heliosheath where the interstellar plasma and magnetic field are deflected around the heliosphere. This interpretation suggests that the polarization is seen where stream lines of the flow and the draped ISMF lines are approximately parallel to each other and perpendicular to the sightline. An ordered magnetic field is required so that grain alignment is not disrupted during the interaction. The filament location is consistent with dust plumes previously predicted to form around the heliosphere. The proposed outer heliosheath location of the polarizing grains can be tested with three-dimensional models that track torques on asymmetric dust grains as they propagate through the heliosheath plasma, and using these models to evaluate grain alignment and the asymmetric extinction of the grains.

Key words: dust, extinction – ISM: magnetic fields – polarization – Sun: heliosphere

1. INTRODUCTION

The Sun's heliosphere and the astrospheres of other stars sweep up interstellar gas and dust as they travel through interstellar clouds. Infrared data show that dusty bow waves, bow shocks, and shells are common around other stars (Peri et al. 2012). Three-dimensional MHD models of the interactions between interstellar dust grains and the heliosphere predict that dust plumes composed of sub-micron grains with high charge-to-mass ratios form around the heliosphere (Slavin et al. 2012). Detection of such a dusty shell around the heliosphere using infrared measurements would be challenging because of the difficulty in separating background emissions from a heliospheric feature.

The center of the "ribbon" arc of energetic neutral atoms (ENAs), discovered by the *Interstellar Boundary Explorer* (*IBEX*) mission, traces the interstellar magnetic field (ISMF) draping over the heliosphere (Funsten et al. 2009, 2013, 2014; McComas et al. 2009; Schwadron et al. 2009; Heerikhuisen et al. 2014). The extraordinary circularity and symmetry of the ribbon supports a hypothesis that the interaction between the heliosphere and the interstellar medium (ISM) involves an ordered magnetic field. Charged interstellar dust grains interacting with the ordered field may polarize starlight and provide an alternate method for sampling a dusty shell around the heliosphere.

The Sun is traveling through an ISM containing partially ionized interstellar gas with low average densities, a magnetic field, and dust (Frisch et al. 2011). The electron density, $\sim$0.03–0.1 cm^{-3}, and magnetic field strength, $\sim 3\,\mu$G, in the surrounding interstellar gas are typical of the magnetoionic medium that contains a structured magnetic field and fills 10%–40% of space (Haffner et al. 2009; Haverkorn 2010). About 0.5%–0.7% of the local interstellar mass density is in charged dust grains (Slavin & Frisch 2008; Krüger et al. 2014). Mapping the structure of the nearby magnetic field requires high-sensitivity measurements of starlight that is polarized by asymmetric dust grains aligned with respect to the foreground ISMF.

This is the fourth study in a global survey of the polarizations of light from nearby stars in order to map the ISMF within 40 pc and compare it with the direction of the ISMF shaping the heliosphere (Frisch et al. 2010, 2012, P. C. Frisch et al. 2015, in preparation, Papers I, II, III). The survey includes stars within $\sim 90^{\circ}$ of the galactic center. A magnetic filament was identified in these polarization data through the linear rotation of their polarization position angles with distance (Paper III). The filament forms a band over 100° long and $\sim 15^{\circ}$ wide in the sky, and extends to within 10 pc of the Sun. Paper III discusses a possible association of this filament

[10] Also at University of Texas, San Antonio, TX, USA.

with the Loop I superbubble. Evidence that this magnetic filament may be associated with the heliosphere is the topic of this paper.

In the diffuse ISM where the ISMF direction is also traced by the Faraday rotation of radio waves and the polarization of synchrotron emission, the optically asymmetric interstellar dust grains that linearly polarize starlight are aligned so that plane of polarization is parallel to the ISMF direction, and is strongest where $\boldsymbol{B} \cdot \boldsymbol{R} = 0$ for magnetic field $\boldsymbol{B}$ and radial sightline $\boldsymbol{R}$ (e.g., Davis & Berge 1968; Lazarian 2007; Andersson et al. 2015). The polarization position angles[11] of the survey data serve as a method for evaluating ISMF direction that is traced by the polarization the data. In Paper III, the filament star polarizations were found to track a separate ISMF direction than the other polarization data in the sample. After the filamanet subset of data was excluded from the analysis of the ISMF direction, the dominant galactic magnetic field in the immediate solar vicinity was found to have a magnetic pole located at $\ell = 36°$, $b = 49°$, ($\pm 16°$) (Paper III, Frisch et al. 2015). This dominant local ISMF direction agrees to within 1σ with the ISMF direction traced by the weighted-mean center of the highly circular *IBEX* ribbon arc (Funsten et al. 2013). The nominal pole directions differ by $7\overset{\circ}{.}6 \pm 16\overset{\circ}{.}2$.

The velocity vectors of interstellar dust and gas flowing into the inner heliosphere are the same. Dust arrives from $\ell = 8°$, $b = 14°(\pm 13°)$ (Frisch et al. 1999; Mann 2010; Belheouane et al. 2012) at a velocity of $-24.5\,\mathrm{km\,s^{-1}}$ (Kimura et al. 2003). Neutral helium arrives from the direction $\ell = 3°$, $b = 16°$, at a velocity of $-26\,\mathrm{km\,s^{-1}}$ (Witte 2004; Bzowski et al. 2012, 2014; Möbius et al. 2012; Katushkina et al. 2014; McComas et al. 2015b; Wood et al. 2015). There is a deficit of low-mass interstellar grains ($<10^{-13}$ gr) in the inner heliosphere compared to the parent interstellar population that is attributed to the action of Lorentz forces on grains with high charge-to-mass ratios in the outer heliosphere and heliosheath regions (Kimura & Mann 1998; Frisch et al. 1999; Linde & Gombosi 2000; Slavin et al. 2012; Sterken et al. 2012). Three-dimensional models of the trajectories of interstellar dust grains interacting with a three-dimensional MHD heliosphere model predict that these excluded grains create shells or plumes of dust around the heliosphere (Slavin et al. 2012).

2. PROPERTIES OF THE MAGNETIC FILAMENT

An ordered component of the local ISMF within 40 pc was originally noticed in Paper II, using the high-sensitivity polarization data set acquired with PlanetPol (Bailey et al. 2010). The distinguishing characteristic of this ordered ISMF was that the polarization position angle in the equatorial coordinate system (θ_{cel}) rotated linearly with the distance of the star. Using an expanded set of stars that included the PlanetPol data, we found a linear relation between the polarization position angle in galactic coordinates, θ_{gal}, and the star distance (Paper III). The stars separated into two groups that had slightly different distance dependences for θ_{gal}, neither of which agreed with the gradient found from θ_{cel} in Paper II. This difference was a clue that the apparent relation between polarization position angle and distance was spurious, and that another factor organized these polarization position angles. The stars showing the regular variation of position angle, θ_{PA}, with distance were found to trace an extended filamentary feature of linearly polarized starlight that extends over 100° in the sky. The polarization data tracing this filament are listed in Table 1, and plotted in Figure 1 in a nose-center ecliptic coordinate system.[12]

In order to search for the organizing principle of the filament, data on three new stars in the region of the filament were collected with DiPol-2 at the UH88 telescope (Piirola et al. 2014). These new data are also listed in Table 1. These polarization data that define the filament were acquired using different instruments at seven observatories; the mean errors of the measurements are not uniform between these different data sets. This extended set of polarization data of 16 stars is used here to search for the controlling factor that creates the alignment of the filament polarizations. Several stars have multiple measurements; all data were used in this analysis. This selection of data is relatively unbiased in the sense that only the three stars observed most recently by DiPol-2, HD 153631, HD 141937, and HD 145518, were observed for the purpose of confirming the filament properties.

The first test performed on the filament polarizations is to determine the direction of the ISMF associated with these polarizations. The best-fitting ISMF to the polarization data in Table 1 was obtained with the method in Papers II and III, where it is assumed that the ISMF direction can be described by a great circle in the sky, and that the best-fitting ISMF direction is the one that minimizes the ensemble of sines of the polarization position angles referenced to the ISMF great circle.[13] A polarization position angle that is perfectly aligned with the ISMF direction will have a position angle of either 0° or 180° when referenced to the ISMF direction, so that the sine of the polarization position angle, θ_{ismf}, is zero. The polarization strengths are not used as the basis for determining the ISMF direction.

Testing this set of position angles against all possible ISMF directions, using a 1° grid and the weighted means of the position angles to evaluate the minimum, yields a best-fitting ISMF direction to the polarizations of the filament stars that is toward $\ell = 357\overset{\circ}{.}3$, $b = 17\overset{\circ}{.}0$ ($\pm 11\overset{\circ}{.}2$). The uncertainties on this direction are obtained from the standard deviation of the polarization position angles calculated with respect to the magnetic field frame, θ_{ismf}, that corresponds to the best-fitting magnetic field pole. An estimate of the magnetic turbulence of this ordered field is obtained by assuming that the uncertainty of $11\overset{\circ}{.}2$ is composed of the root mean square of the turbulent field component and the mean uncertainty of the position angle measurements, $\boldsymbol{\Delta}\theta_{\mathrm{PA}} = 5\overset{\circ}{.}6$, so that the "turbulent" component of the position angles is approximately $\pm 9\overset{\circ}{.}6$.

The surprising result of best-fitting ISMF direction to the filament polarizations is that it is within $6\overset{\circ}{.}7 \pm 11\overset{\circ}{.}2$ of the upwind velocity vector of the primary interstellar neutral helium flow into the heliosphere, which arrives from the direction of $\ell = 3°$, $b = 16°$ (or $\lambda = 255°$, $\beta = 5°$ in ecliptic

[11] The polarization position angle is the angle between the plane of polarization of the E-vector and the north pole, and labeled positive for rotations of the postion-angle meridian toward larger longitudes.

[12] The heliosphere nose is defined by the direction of inflowing neutral interstellar helium atoms, $\lambda = 255°$, $\beta = 5°$, or $\ell = 4°$, $b = 15°$ (McComas et al. 2015b).

[13] In the context of the software, this assumption is implemented by rotating the coordinate system into a 1° grid covering the sky to find the direction that best-matches the rotated polarization position angles. No assumption is made about the three-dimensional distribution of the ISMF since the polarizing dust screens can be anywhere in the sightline. See P. C. Frisch et al. (2015, in preparation) for more details.

coordinates, e.g., McComas et al. 2015b). The coincidence between the directions of ISMF vector and the velocity vector of neutral interstellar gas flowing into the heliosphere suggests that the filament may be related to the heliosphere, and that the filament axis may trace a feature of the heliosphere.

The major axis of the filament axis can be approximated by fitting a line through the galactic coordinates of the stars. The best-fitting line corresponds to $\ell = 25.^{\circ}118(\pm 1.^{\circ}258) - 0.^{\circ}139\ (\pm 0.^{\circ}037) \times \delta\ \ell$, with a reduced χ^2 of 1.14; here $\delta\ell$ is the difference between the star galactic longitude and the end point of the polarization filament at $\ell = 316^{\circ}$ (Table 1). The long axis of the filament is shown as the gray line in Figure 2.

The angle between the filament axis and the ***BV*** plane of the heliosphere is $80^{\circ} \pm 14^{\circ}$, so that the filament axis and ***BV*** plane are perpendicular. The ***BV*** plane, projected as the gray dashed line in Figure 2, is the plane formed by the ISMF (***B***) and neutral interstellar wind velocity (***V***) vectors that shape the heliosphere (Opher et al. 2009; Pogorelov et al. 2009). For the magnetic field direction (***B***) we use the center of the *IBEX* ribbon arc at 4.3 keV (Funsten et al. 2013). At this energy ENAs will have longer mean free paths than those at lower energies, so that this direction extends further into the ISMF than the directions from lower energies. The interstellar velocity (***V***) is given by the velocity vector of neutral interstellar helium flowing through the heliosphere (McComas et al. 2015b). Ribbon models indicate that the ribbon center is within 5° of the true ISMF direction for likely field strengths of 3 μG (Heerikhuisen et al. 2014).

A range of heliospheric data indicate that the ***BV*** plane plays a fundamental role in organizing the interaction between the ISM and the heliosphere. Charge exchange coupling between interstellar neutrals and ions cause an offset of the neutral gas flow along a direction that is parallel to the ***BV*** plane; examples are the $4.^{\circ}7$ deflection of the interstellar hydrogen flow from the benchmark He° flow direction (Lallement et al. 2010), and the offset of the secondary helium population (a "warm breeze," Kubiak et al. 2014, Figure 2). The ***BV*** plane also plays an organizing role in the spectral dependence of the ribbon symmetry, with ENAs (Funsten et al. 2014), and organizes the heliosphere asymmetries (Figure 3).

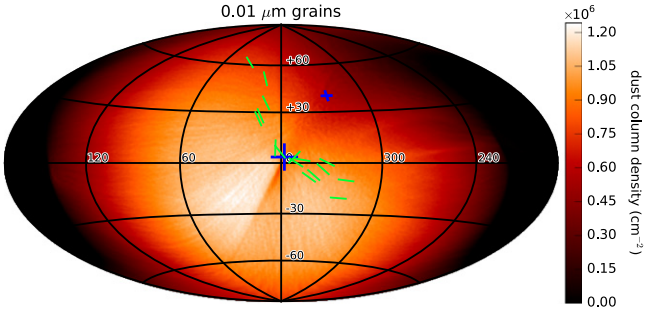

Figure 1. Filament star polarizations (green bars) are shown plotted against the modeled column densities of radius 0.01 μm interstellar dust grains interacting with the heliosphere. The small and large blue crosses indicate the direction of the *IBEX* ribbon ISMF and inflowing interstellar gas. The horizontal axis coincides with the ecliptic plane and the image is centered on the heliosphere nose defined by the inflowing ISM. The color coding shows the column density for 0.01 dust micron grains out to a distance of 400 AU. Color coding is based on the true column density (cm^{-2}) for the grains for a gas-to-dust ratio of 150. The dust distribution is from the dust trajectory models of Slavin et al. (2012).

Figure 1 plots the filament polarizations over a simulation of the column densities of 0.01 μm interstellar dust grains within 400 AU from Slavin et al. (2012, S12). The Figure is an

Table 1
Stars Tracing Magnetic "Filament"

Star		Coordinates ℓ, b (deg)	Distance (pc)	Spec.	Polarization[a] (10^{-5})	θ_{gal} (deg)	Ref.[b]
Data Used in Paper III[c]							
HD 131977	⋯	338, 34	6	K4 V	55.4 ± 24.0	99.2 ± 12.3	LNA
HD 161797	⋯	52, 26	8	G5 IV	0.93 ± 0.21	92.3 ± 6.7	PP
HD 172167	α Lyr	67, 19	8	A0 Va	1.72 ± 0.1	104.7 ± 1.4	PP, W
HD 159561	α Oph	36, 23	14	A5 III V	2.34 ± 0.2	96.4 ± 2.4	PP, W
HD 120467	⋯	320, 38	14	K1 III	77.0 ± 23.0	120.9 ± 8.6	San
HIP 82283	⋯	4, 18	18	G6 III	113.0 ± 25.0	100.1 ± 6.3	San
HD 144253	⋯	353, 23	19	K3 V	13.0 ± 3.0	115.2 ± 7.5	NOT
HD 119756	⋯	316, 29	19	F2 V	90.0 ± 35.0	122.4 ± 10.6	Hls
HD 130819	⋯	340, 38	24	F3 V	6.0 ± 3.0	114.9 ± 14.5	NOT
HD 134987	⋯	339, 27	26	G6 IV-V	14.0 ± 2.0	100.6 ± 4.5	NOT
HD 136894	⋯	340, 24	28	G8 V	14.0 ± 4.0	106.6 ± 8.0	NOT
HD 161096	⋯	29, 17	25	K2 III	3.2 ± 0.2	90.9 ± 1.9	PP, W
HD 161868	γ Oph	28, 15	29	A1 V	4.1 ± 0.3	91.1 ± 2.1	PP, W
New Data from DiPol-2 at UH88[d]							
HD 153631	⋯	7, 17	26	G0 V	9.0 ± 0.9	59.8 ± 3.1	UH[e]
HD 141937	⋯	352, 27	33	G2 V	7.9 ± 1.0	137.0 ± 4.3	UH
HD 145518	⋯	356, 24	33	G0.5 V	5.2 ± 1.1	5.2 ± 1.1	UH

Notes.
[a] The units are degree of polarization.
[b] References: LNA—data collected at LNA Picos dos Dios and listed in Frisch et al. (2012) or P. C. Frisch et al. (2015, in preparation); W—Wiktorowicz data from Lick observatory (2014, private communication); PP—PlanetPol data from Bailey et al. (2010); NOT—Paper II; San—LNA Picos dos Dios data from Santos et al. (2011); Hls—compiled data from different sources in Heiles (2000). UH—data collected with the UH88 and presented in this paper.
[c] P. C. Frisch et al. (2015, in preparation).
[d] These data were obtained with DiPol-2 on the University of Hawaii 2.2 m telescope in 2014 June and July.
[e] HD 153631 was also observed by NOT in 2010 (Frisch et al. 2012), giving $P = 5 \pm 3 \times 10^{-5}$ degree of polarization and $\theta_{gal} = 61.^{\circ}2 \pm 13.^{\circ}40$.

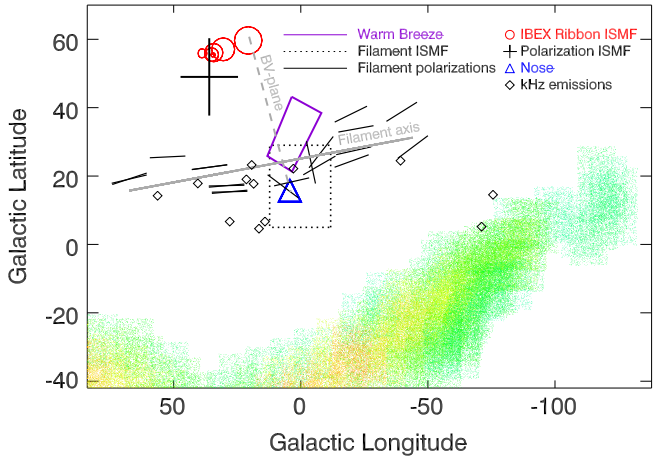

Figure 2. The polarizations of the filament stars are compared to markers of the outer heliosheath region or beyond. Those polarizations, and the best-fitting magnetic field direction to those polarizations $B_{\rm filament}$, are plotted in galactic coordinates as black bars and the dotted-line box (which outlines the uncertainty range). The uncertainties on $B_{\rm filament}$ overlap the upwind direction of the primary interstellar He° atoms (blue triangle) and the uncertainty range of the inflowing warm He° breeze (purple box, solid line). The ISMF directions from the centers of the *IBEX* ribbon arc for the five energy bands of *IBEX*-HI (Funsten et al. 2013) are plotted as red open circles, with the size of the circle increasing with energy. The black diamonds represent the locations of the low frequency outer heliosheath 2–3 kHz emissions reported in Kurth & Gurnett (2003). The magnetic field direction that dominates polarization data ($B_{\rm CLIC}$, large black cross, P. C. Frisch et al. 2015, in preparation) overlaps the ISMF found from the *IBEX* ribbon. The dashed and solid gray lines show the locations of the ***BV*** plane and the axis of the filament, respectively. The lines enclose an angle of 80° ± 14° and are perpendicular to each other. The fluxes of the *IBEX* ribbon for the ~1.1 keV energy band are plotted on the color scale, with the highest fluxes plotted as red and the lowest fluxes plotted in green (see Figure 4 of Schwadron et al. 2014).

ecliptic projection centered on the nose of the heliosphere, defined by the inflowing interstellar helium gas. Slavin et al. (2012, S12) modeled the trajectories of interstellar compact silicate grains through the 3D MHD heliosphere models of Pogorelov et al. (2009). These models were successfully used by Schwadron et al. (2009) to show that the *IBEX* ribbon appears in sightlines that are perpendicular to the ISMF draping over the heliosphere, i.e., where $\boldsymbol{B} \cdot \boldsymbol{R} = 0$ for magnetic field vector $\boldsymbol{B}$ and radial direction $\boldsymbol{R}$. The models include an ISMF direction that is within ~17° of the interstellar field direction traced by the weighted center of the *IBEX* ribbon arc.[14] Densities of 0.01 μm interstellar grains within ~400 AU of the Sun are shown in Figure 1 based on these models. The filament crosses the heliosphere nose at the plot center and reaches high latitudes on the port side of the heliosphere at HD 172167, and low latitudes on the starboard side of the heliosphere at HD 119756 (borrowing nautical terminology[15]). The ***BV*** plane controls the symmetry of the cloud of interstellar dust grains interacting with the heliosphere, and the asymmetry of the polarization filament about the ***BV*** plane is evident. The filament is slightly more twisted toward the vertical direction in the north and port side of the heliosphere compared with the starboard side in this simulation.

3. DISCUSSION

3.1. Possible Origin of Filament Polarizations in Outer Heliosheath

The agreement between the ISMF direction of the filament polarizations and the velocity vector of interstellar material flowing through the heliosphere, the perpendicularity between the ***BV*** plane and the filament axis, and the low level of magnetic turbulence in the filament, suggest that the filament polarizations may be associated with the deflection of charged grains, the ISMF, and interstellar plasma around the heliosphere in the outer heliosheath regions.

Interstellar nanograins with large charge-to-mass ratios (Q/m) are deflected in the outer and inner heliosheath regions, and throughout the heliosphere (Frisch et al. 1999; Kimura & Mann 1999; Linde & Gombosi 2000; Czechowski & Mann 2003; Mann & Czechowski 2004; Slavin et al. 2012;

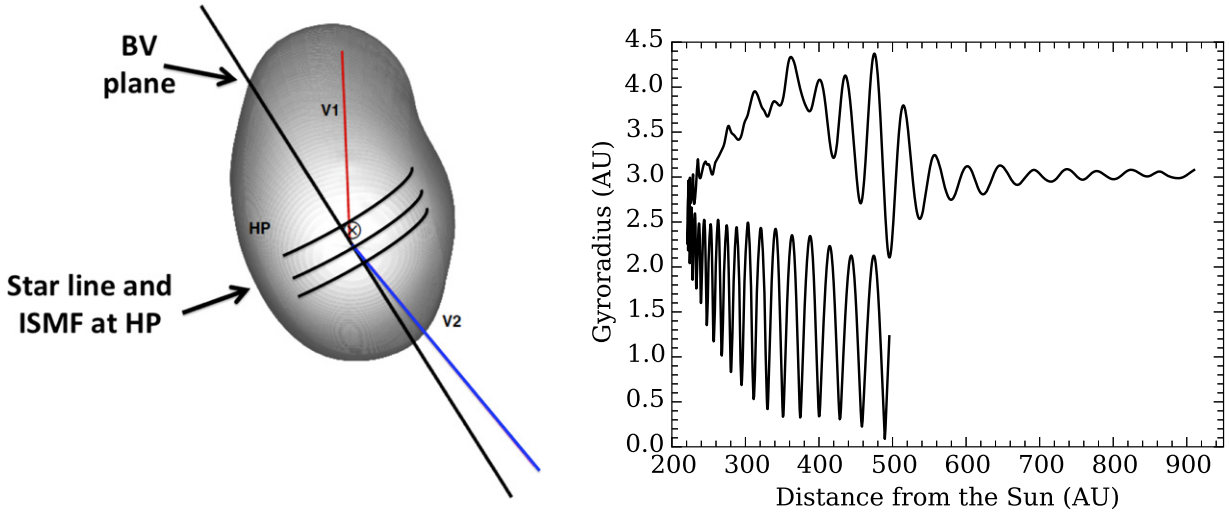

Figure 3. Left: cartoon showing the ***BV*** plane and filament star line plotted against a frontal view of the heliopause, i.e., as viewed from the upwind direction. The heliopause cartoon is borrowed from the MHD model displayed in Figure 1(a) of (Pogorelov et al. 2011). The ***BV*** plane corresponds to the hydrogen deflection plane displayed by (Pogorelov et al. 2011) in Figure 1(a). The orientation of the filament star line is displayed by the draped lines. The filament orientation is perpendicular to the ***BV*** plane, and the filament magnetic field is directed toward the upwind velocity of interstellar neutrals, suggesting that a heliospheric origin requires the filament to form where the interstellar dust and magnetic field are fully deflected at the heliosphere nose. Right: modeled trajectory of an interstellar grain such as may generate the polarization is displayed on the right, for a compact dust grain with radius 0.01 μm approaching the heliosphere nose from the upwind direction. The grain gyroradius varies as the grain charge is modified by interactions with the heliospheric radiation and plasma components, until the grain is finally deflected around the heliopause along with the interstellar plasma and magnetic field (see Slavin et al. 2012 for modeling details).

Sterken et al. 2012; Krüger et al. 2014). Most grain trajectory simulations have assumed compact grains. Tiny grains are subject to the small particle effect, where the efficiency of secondary ejection of electrons is enhanced (Kimura & Mann 1998). Porous or fluffy grains that consist of aggregates of tiny grains are also subject to this effect, which leads to higher grain charges and increases the average mass of the outer heliosheath grains above the predicted levels for compact grains (Ma et al. 2013). These deflected grains are candidates for the polarizing dust grains in the filament.

The mass distributions of the interstellar dust grains observed within 5 AU of the Sun exhibit a deficit of low mass grains, $<10^{-13}$ gr (Frisch et al. 1999; Landgraf et al. 2000; Krüger et al. 2014), when compared with the nominal power-law interstellar distribution of Mathis et al. (1977). The deficit of small grains is attributed partly to the "filtration" of grains with large values of Q/m that couple to the interstellar plasma and magnetic field that is swept around the heliopause (Frisch et al. 1999; Kimura & Mann 1999; Linde & Gombosi 2000; Czechowski & Mann 2003; Mann & Czechowski 2004; Slavin et al. 2012; Krüger et al. 2014).

The perpendicular relation between the filament axis and the ***BV*** plane would be an outcome of the Lorentz force on the grains. Nanograins experience additional charging in the outer heliosheath due to collisions with the heated compressed interstellar plasma and enhanced radiation field, with the maximum differential increase in the surface potential of the grains occurring for the smallest grains (Figure 2 of S12). S12 showed that the surface potentials of compact interstellar silicate grains in heliosheath regions are enhanced by an order of magnitude compared to values in the surrounding ISM. As the dust grains approach the heliosphere from the distant ISM, Lorentz forces act to displace grains into directions that are perpendicular to the ***BV*** plane. The action of the Lorentz force on grains with large Q/m the grains naturally explains the orientation of the filament axis with respect to the ***BV*** plane. Figure 3 shows the gyroradius of a 0.01 μm radius interstellar grain propagating through the outer heliosheath region, and as the grain is deflected around the heliopause by the Lorentz force; the grain trajectory model is based on the simulations in S12.

The $\sim 15^{\circ}$ width of the filament is not yet explained. Since all of the smallest grains are deflected, the filament width must depend on the detailed configuration of the heliopause, the grain charging that occurs in the outer heliosheath, and the strength of the Lorentz force. The dust plumes in the models of S12 (Figure 13 of S12, left) have a limited width that is similar to the filament width, and a similar spatial orientation perpendicular to the ***BV*** plane. Those dust plumes therefore provide a plausible model for the polarization filament location, provided that the efficiency of polarization can be explained.

If the filament has a heliospheric origin, then the second characteristic of the filament, that the ISMF is directed toward the inflow vector of interstellar neutrals, implies that the filament forms where the interstellar ion and dust streamlines are parallel to each other and to the localized ISMF direction. The surrounding interstellar gas consists of about 23% ions and 77% neutral atoms (Slavin & Frisch 2008). The collisional mean-free-path in the ISM approaching the heliosheath regions is ~330 AU (Spangler et al. 2011), and is similar to the thickness of the plasma density ramp outside of the heliopause (Zank et al. 2013).[16]

Interstellar ions and neutrals follow different trajectories in the outer heliosheath. Ions are deflected around the heliopause, and the neutrals propagate through the plasma, with some loss due to the formation of ENAs. The frozen-in interstellar field becomes fully deflected where the ions decouple from the inflowing interstellar neutrals at the heliopause, so that the deflected plasma streamlines and magnetic field should be directed toward the undeflected neutral velocity vector. A correspondence between the ISMF direction and the He° flow velocity suggests that the direction of the draped ISMF has twisted into the direction of the deflected gas flow (e.g., see Opher & Drake 2013).

An important requirement is that the dust grains remain aligned with respect to the ISMF direction during the deflection of the dust flow at the heliopause. The organized set of filament polarizations must be tracing an organized magnetic field that has a minimal turbulence. The recent in situ measurements of the magnetic field in the inner and outer heliosheath regions with instruments on board *Voyager 1* support an ordered field in the outer heliosheath (Burlaga et al. 2013, 2014; Burlaga & Ness 2014). *Voyager 1* crossed into the ISMF in mid-2012 and found a more ordered magnetic field in the outer heliosheath than had been seen in the inner heliosheath, with less turbulence, and a maximum standard deviation of the magnetic field strength that was 3% of the total field strength. In contrast, in the inner heliosheath the maximum standard deviation of the compressive turbulence (corresponding to variations in magnetic field strength) was 36% of the total field strength suggesting that the inner heliosheath is unlikely to be the origin of the polarizations.

The low level of interstellar field turbulence in the outer heliosheath found by *Voyager 1* suggests that high magnetic pressures will concentrate the nanograins in the outer heliosheath and increase the efficiency of the grains to linearly polarize light. However, Rayleigh–Taylor instabilities can disrupt the heliopause and allow the charged interstellar particles to penetrate into the inner heliosheath (Borovikov & Pogorelov 2014; Avinash et al. 2014). The blunt heliosphere inferred from *Voyager* data of the neutral current sheet (Burlaga & Ness 2014) and plasma flow (Richardson & Decker 2014), and the extended high-pressure region at the heliosphere nose seen in *IBEX* data (McComas et al. 2014a) and predicted by heliosphere models (Pogorelov et al. 2011), is going to affect the draping of the ISMF over the heliosphere in ways that are not yet fully understood.

A "cartoon" illustrating the geometric relation between the filament polarizations and the heliosheath is shown in Figure 3; the surface of the heliopause is from the MHD model of Pogorelov et al. (2011, Figure 1), where the ***BV*** plane and *Voyager* trajectories are also shown. The filament orientation perpendicular to the ***BV*** plane is displayed, with the filament located close to the heliopause on the upwind side. The

[14] The galactic coordinates of the weighted mean center of the *IBEX* ribbon arc are $\ell = 36.^{\circ}7 \pm 2.^{\circ}1$, $b = 56.^{\circ}0 \pm 0.^{\circ}6$ (Funsten et al. 2013; Frisch et al. 2014).

[15] In nautical usage, port and starboard are referenced to the bow of a ship. Using an *xyz* right-handed cartesian coordinate system, the *x*-axis is directed toward the bow, the *y*-axis is directed toward the port side and the *z*-axis points "up" toward the opposite direction of the gravitational force. By analogy, for the heliosphere the nose-direction of the heliosphere corresponds to the *x*-axis, the *y*-axis is directed toward the port side of the heliosphere, and the *z*-axis, pointing north, completes the right-handed coordinate system.

[16] The inner heliosheath thickness found from *Voyager 1* and *IBEX* data is ~27 AU (Hsieh et al. 2010; Gurnett et al. 2013).

hypothesized local distortion of the magnetic field direction parallel to the filament and heliopause is also illustrated.

3.2. Alignment of the Filament with respect to the IBEX Ribbon

For starlight that is linearly polarized in the ISM, a polarization position angle that is aligned with the ISMF direction will yield the strongest polarizations where the ISMF is perpendicular to the radial sightline, e.g., where $\boldsymbol{B} \cdot \boldsymbol{R} = 0$. In contrast, the filament polarizations trace a magnetic field direction that is directed toward the upwind velocity of neutral interstellar gas instead of the ISMF direction corresponding to the center of the *IBEX* ribbon arc, ∼48° away from the gas velocity. Our hypothesis is that the polarization filament is visible where the dust grains are entrained in the ISMF that has been deflected around the heliosphere, so that polarizations would be strongest where the field lines are quasi-perpendicular to the sightline for otherwise-equal conditions.

Comparison between MHD heliosphere models and the *IBEX* ribbon location show that the ∼1 keV ribbon is observed in sightlines where the ISMF becomes perpendicular to the sightline as the field drapes over the heliosphere, i.e., where $\boldsymbol{B} \cdot \boldsymbol{R} = 0$ (McComas et al. 2009; Schwadron et al. 2009; Chalov et al. 2010; Heerikhuisen et al. 2010; Schwadron & McComas 2013). Figure 2 shows that the filament polarizations are roughly parallel to the *IBEX* ribbon.

There is no consensus on the formation scenario for the *IBEX* ribbon, although the original model where the ribbon is viewed along sightlines perpendicular to the ISMF draping over the heliosphere is generally accepted (for a review see McComas et al. 2014b). Formation from secondary ENA's upstream of the heliopause is currently the leading contender for explaining the ribbon. In these models the ribbon ENAs form upstream of the heliopause where charge-exchange between interstellar neutral hydrogen atoms and the pickup-ion plasma, which came from the neutralized outward moving solar wind, creates ENAs. These ENAs propagate back toward *IBEX* if the ion pitch angles retain the dominant radial momentum of the original outward flowing particles. Models relying on secondary pickup ions to generate the ribbon place the origin 50–100 AU upstream of the heliopause (Heerikhuisen & Pogorelov 2011) up to several hundred AU. Presumably the interstellar ions and the dust grains with small Q/m will couple more tightly to the deflected ISMF than do the pickup ions that create the neutral ENAs, so that the polarization filament would appear at the region where the small Q/m grains are fully deflected rather than precisely where $\boldsymbol{B} \cdot \boldsymbol{R} = 0$.

3.3. Are Outer Heliosphere Grains enough to Polarize Starlight?

Interstellar column densities in the outer heliosheath are expected to be lower than total column densities toward the nearest stars. The gas column densities in the outer heliosheath are only 0.06%–0.9 of the total interstellar column densities toward the nearby upwind star 36 Oph (6 pc), if the hydrogen-wall and interstellar data in Wood et al. (2000) are used to benchmark this relation. For an average hydrogen-wall density of $n(H^o) = 0.25\,cm^{-3}$, the three-component hydrogen-wall model of Wood et al. (2000) suggests an outer heliosheath thickness of ∼100 AU toward 36 Oph. If the filament polarizations are formed in an outer heliosheath region that is on the order of 100 AU thick, then either grain alignment is significantly more efficient in the heliosheath than in the local ISM, or an unknown factor such as foreground depolarization is reducing the interstellar polarizations of nearby stars.

The outer heliosheath physical conditions differ from those in the ISM upstream of the heliosphere. Although detailed models are required to evaluate the alignment of grains propagating through the outer heliosheath, the factors that increase polarization efficiency in this relatively thin region can be described qualitatively. These factors include higher grain surface potentials, enhanced strength and asymmetry of the radiation field, enhanced magnetic field strengths, low levels of magnetic turbulence, and the absence of foreground depolarizations, all when compared to the values in the local ISM. The presence of fluffy or porous grains, which are more sensitive to secondary electron ejection than compact grains, further enhancing grain alignment.

Self-consistent simulations of compact interstellar grains interacting with the heliosheath regions show that surface potentials of the grains increase by up to an order of magnitude in the outer heliosheath, depending on grain radius (S12). The higher Q/m values will increase grain charge and the Lorentz force on grains, and minimize possible collisional disruption of the grain alignment.

Radiative torques play a role in grain alignment in interstellar clouds (Andersson et al. 2015). Hoang & Lazarian (2014) have modeled the polarizations expected for the very local ISM, taking into account that radiative torques on optically asymmetric grains play a dominant role in grain alignment in the warm local ISM where gas column densities are typically $10^{17.7}$–$10^{18.7}\,cm^{-2}$. Their models were able to account for polarization strengths as low as 0.002%, depending on the total column density of the gas. The polarization strengths of the filament stars range from 0.0032% to 0.1% (Table 1), however the filament polarizations probably form over a column that is <0.002 times the length of the column of interstellar polarizations. Radiative torques that enhance grain alignment will become of increasing importance as grains approach the heliopause and experience a stronger, more asymmetric, and more energetic radiation field (see Figure 3 in S12).

As the ISMF strength increases as field is compressed against the heliopause by the solar motion through the surrounding ISM, interstellar dust grains will couple more tightly to the ISMF because of smaller gyroradii. The interstellar field strength is enhanced by factors of 3 or more outside of the heliopause in the models used by Slavin et al. (2012). *Voyager*1 found that field strengths in the outer heliosphere reach 6 μG, which suggests a compression factor of 2 when compared to the 3 μG field strength of the interstellar cloud around the heliosphere (Slavin & Frisch 2008; Schwadron et al. 2011; Burlaga & Ness 2014).

Polarizations are not additive in the ISM since foreground clouds may depolarize polarized light (Davis & Berge 1968; Serkowski et al. 1975). There is no information on foreground depolarization in the local ISM so the local significance of this effect is unknown. However, when compared to interstellar values, there is unlikely to be foreground depolarization of polarizations originating in the outer heliosphere. In principle the absence of depolarization will further increase the efficiency of heliosheath polarizations above those in the ISM.

A significant enhancement of polarizations compared with previous simulations of polarization efficiencies may arise from

the physical structure of the excluded grains, and whether they are compact or porous aggregates ("fluffy"). Photoionization models of interstellar gas around the heliosphere show the presence of olivine silicates and the absence of carbonaceous grains (Slavin & Frisch 2008). The grain trajectory models that predict dust plumes around the heliosphere (S12) are based on compact olivine silicate grains with densities of 3.3 gr cm^{-3}. In situ measurements by Stardust found interstellar grains with very low volume densities, <0.07 gr cm^{-3} (Westphal & the Stardust Team 2014). Recently, V. J. Sterken et al. (2015, in preparation) found an indication of porous grains from comparisons of the flow directions of interstellar grains in 16 years of interstellar dust measurements from *Ulysses*, such as was proposed in earlier discussions (cf. Mann 2010). In situ measurements of interstellar dust in the inner heliosphere have found large grains with masses 2×10^{-10} gr (radii ~ 2 μm for compact grains, Frisch et al. 1999; Slavin et al. 2012; Krüger et al. 2014). These heliospheric large grains are similar in size to the large micron-sized aggregate grains that are observed in the cores of dense interstellar clouds (Pagani et al. 2010; Santos et al. 2014). Outside of dense clouds the large grains couple to the interstellar gas over pathlengths of ~50–100 pc (Grün & Landgraf 2000), and the local population of large grains may be enriched by porous dust grains from fragmented dense clouds.

Porous grains have larger cross-sections than the canonical compact grains that have been used for modeling the dust–heliosphere interactions. Ma et al. (2013) have modeled the grain charging of aggregate grains and found that the surface potentials of porous grains is increased by 30% or more in the outer heliosheath, which allows a stronger coupling between the dust and deflected heliosheath plasma and magnetic field. Aggregate porous grains have higher charges than compact grains, and so are deflected differently. The high end of the cutoff masses for the deflected grains is increased, so that more high-mass grains are prevented from entering the heliosphere and the masses of the dust plumes would be enhanced compared to models based on compact grains. Hoang & Lazarian (2014) find that larger grains are more sensitive to radiative torques, so that the polarizations of large fluffy grains should be further enhanced over those of compact grains in the outer heliosheath.

4. CONCLUDING REMARKS

A filament of polarized starlight has been discovered within 10 pc of the heliosphere. The filament stars were initially identified from the rotation of polarization position angles with star distance. This study links these polarizations to the outer heliosheath regions where previous simulations indicate that interstellar nanograins are deflected in plume-like features around the heliosphere. The filament polarizations show three primary observational properties: (1) the best-fitting ISMF vector to the filament polarization position angles coincides with the upwind velocity vector of interstellar neutrals flowing into the heliosphere. (2) The axis of this 100°-long filament is perpendicular to the ***BV*** plane, formed by the interstellar and magnetic and gas-velocity vectors, that shapes the heliosphere. (3) A contribution of $\pm 9\overset{\circ}{.}6$ to the dispersion of the polarization position angles can be attributed to magnetic turbulence.

We propose that the filament is formed in the outer heliosheath, where the ISMF and interstellar plasma are deflected around the heliosphere. The polarizations would be found where the flow streamlines and draped ISMF are approximately parallel to each other, and roughly perpendicular to the ***BV*** plane and sightline. However, although the filament traces several physical properties of the outer heliosheath, the difference in the thickness of the heliosheath compared with normal interstellar sightlines suggests that grain alignment mechanisms in the outer heliosheath would have to be more efficient than in the general ISM for such an origin.

An outer heliosphere origin for the filament can be tested by evaluating the propagation of porous interstellar dust grains through MHD models of the dynamically evolving outer heliosheath plasma and magnetic fields. Alignment efficiency in the outer heliosheath, compared to the ISM, would be augmented by increased grain charging, radiative torques, and stronger magnetic field strengths. Porous interstellar grains will substantially increase the mass and number of deflected interstellar grains above values for compact grains. The models will need to keep track of magnetic, collisional, and radiative torques on the grains in order to evaluate grain alignment and the asymmetric grain opacity that causes polarization. Filament properties that need to be explained include the filament width, the connection between the filament ISMF vector and neutral He flow vector, and detailed modeling of grain alignment mechanisms and polarization efficiencies for porous grains.

The properties of the outer heliosheath are poorly known. While *IBEX* and the two *Voyager* missions have provided essential data on the outer heliosphere, data on the vector motion of the outer heliosheath plasma are not presently available because the *Voyager 1* plasma instrument is not operational and *Voyager 2* has not yet reached the heliopause (e.g., Richardson & Decker 2014). If an outer heliosheath origin for the filament polarizations is confirmed by theoretical modeling, a new diagnostic of the outer heliosheath will become available. This diagnostic would have the unique property of allowing the outer heliosheath to be monitored using ground-based observations. This convergence between interstellar dust data and heliosheath science would be useful for understanding the interactions between astrospheres around external stars and the ISM, heliosphere-related foregrounds to the cosmic microwave background, and the time-variable flux of interstellar grains into the inner heliosphere and terrestrial atmosphere.

This research has been partly supported by the NASA Explorer program through support for the *IBEX* mission, and by the European Research Council Advanced Grant HotMol (ERC-2011-AdG 291659).

Note added in proof. The forerunner stars of the filament were originally selected in Paper II because they traced the upper envelope of the polarization strength vs. distance relation over an exceptional region of the sky that had been identified in the PlanetPol study (Bailey et al. 2010). Those upper-envelope stars were then found to have equatorial polarization position angles that rotated linearly with distance. With the extended data set and larger spatial coverage of Paper III, the relation between polarization position angle and distance was found to be spurious since it varied with the coordinate system of the position angles. The result led to the new analysis here linking the organizing principle of the filament to the heliosphere properties, rather than to the distance of the star itself.

REFERENCES

Andersson, B.-G., Lazarian, A., & Vaillancourt, J. E. 2015, ARA&A, in press
Avinash, K., Zank, G. P., Dasgupta, B., & Bhadoria, S. 2014, ApJ, 791, 102
Bailey, J., Lucas, P. W., & Hough, J. H. 2010, MNRAS, 405, 2570
Belheouane, S., Zaslavsky, A., Meyer-Vernet, N., et al. 2012, SoPh, 281, 501
Borovikov, S. N., & Pogorelov, N. V. 2014, ApJL, 783, L16
Burlaga, L. F., & Ness, N. F. 2014, ApJ, 784, 146
Burlaga, L. F., Ness, N. F., Florinski, V., & Heerikhuisen, J. 2014, ApJ, 792, 134
Burlaga, L. F., Ness, N. F., & Stone, E. C. 2013, Sci, 341, 147
Bzowski, M., Kubiak, M. A., Hlond, M., et al. 2014, A&A,
Bzowski, M., Kubiak, M. A., Möbius, E., et al. 2012, ApJS, 198, 12
Chalov, S. V., Alexashov, D. B., McComas, D., et al. 2010, ApJL, 716, L99
Czechowski, A., & Mann, I. 2003, A&A, 410, 165
Davis, L. J., & Berge, G. L. 1968, Evidence for Galactic Magnetic Fields (Chicago, IL: Univ. Chicago Press), 755
Frisch, P. C., Andersson, B., Berdyugin, A., et al. 2010, ApJ, 724, 1473
Frisch, P. C., Andersson, B.-G., Berdyugin, A., et al. 2012, ApJ, 760, 106
Frisch, P. C., Berdyugin, A., Funsten, H. O., et al. 2015, in Proc. 13th Annual Int. Astrophysics Conf.: Voyager, IBEX, and the Interstellar Medium, Journal of Physics Conference Series Vol. 577, ed. G. P. Zank (Bristol: IOP Publishing), 012010
Frisch, P. C., Dorschner, J. M., Geiss, J., et al. 1999, ApJ, 525, 492
Frisch, P. C., Redfield, S., & Slavin, J. 2011, ARA&A, 49
Funsten, H. O., Allegrini, F., Crew, G. B., et al. 2009, Sci, 326, 964
Funsten, H. O., Bzowski, M., Cai, D. M., et al. 2014, ApJ, 215, 13
Funsten, H. O., DeMajistre, R., Frisch, P. C., et al. 2013, ApJ, 776, 30
Grün, E., & Landgraf, M. 2000, JGR, 105, 10291
Gurnett, D. A., Kurth, W. S., Burlaga, L. F., & Ness, N. F. 2013, Sci, 341, 1489
Haffner, L. M., Dettmar, R. J., Beckman, J. E., et al. 2009, RvMP, 81, 969
Haverkorn, M. 2010, in ASP Conf. Ser. 438, The Dynamic Interstellar Medium: A Celebration of the Canadian Galactic Plane Survey, ed. R. Kothes, T. L. Landecker, & A. G. Willis (San Francisco, CA: ASP), 249
Heerikhuisen, J., & Pogorelov, N. V. 2011, ApJ, 738, 29
Heerikhuisen, J., Pogorelov, N. V., Zank, G. P., et al. 2010, ApJL, 708, L126
Heerikhuisen, J., Zirnstein, E. J., Funsten, H. O., Pogorelov, N. V., & Zank, G. P. 2014, ApJ, 784, 73
Heiles, C. 2000, AJ, 119, 923
Hoang, T., & Lazarian, A. 2014, MNRAS, 438, 680
Hsieh, K. C., Giacalone, J., Czechowski, A., et al. 2010, ApJL, 718, L185
Katushkina, O. A., Izmodenov, V. V., Wood, B. E., & McMullin, D. R. 2014, ApJ, 789, 80
Kimura, H., & Mann, I. 1998, ApJ, 499, 454
Kimura, H., & Mann, I. 1999, EP&S, 51, 1223
Kimura, H., Mann, I., & Jessberger, E. K. 2003, ApJ, 582, 846
Krüger, H., Strub, P., Sterken, V. J., & Grün, E. 2014, ApJ, submitted
Kubiak, M. A., Bzowski, M., Sokół, J. M., et al. 2014, ApJS, 213, 29
Kurth, W. S., & Gurnett, D. A. 2003, JGR, 108, 2
Lallement, R., Quémerais, E., Koutroumpa, D., et al. 2010, in 12th Int. Solar Wind Conf. 1216: The Sun, the Solar Wind, and the Heliosphere, ed. M. Paz Miralles & J. Sanchez Almeida (Melville, NY: AIP), 555
Landgraf, M., Baggaley, W. J., Grün, E., Krüger, H., & Linkert, G. 2000, JGR, 105, 10343
Lazarian, A. 2007, JQSRT, 106, 225
Linde, T. J., & Gombosi, T. I. 2000, JGR, 105, 10411
Ma, Q., Matthews, L. S., Land, V., & Hyde, T. W. 2013, ApJ, 763, 77
Mann, I. 2010, ARA&A, 48, 173
Mann, I., & Czechowski, A. 2004, in AIP Conf. Proc. 719, Physics of the Outer Heliosphere, ed. N. Florinski, N. V. Pogorelov, & G. P. Zankpage (Melville, NY: AIP), 53
Mathis, J. S., Rumpl, W., & Nordsieck, K. H. 1977, ApJ, 217, 425
McComas, D. J., Allegrini, F., Bochsler, P., et al. 2009, Sci, 326, 959
McComas, D. J., Allegrini, F., Bzowski, M., et al. 2014a, ApJS, 213, 20
McComas, D. J., Bzowski, M., Frisch, P. C., et al. 2015, ApJ, 801, 28
McComas, D. J., Lewis, W. S., & Schwadron, N. A. 2014b, RvGeo, 52, 118
Möbius, E., Bochsler, P., Bzowski, M., et al. 2012, ApJS, 198, 11
Opher, M., Bibi, F. A., Toth, G., et al. 2009, Natur, 462, 1036
Opher, M., & Drake, J. F. 2013, ApJL, 778, L26
Pagani, L., Steinacker, J., Bacmann, A., Stutz, A., & Henning, T. 2010, Sci, 329, 1622
Peri, C. S., Benaglia, P., Brookes, D. P., Stevens, I. R., & Isequilla, N. L. 2012, A&A, 538, A108
Piirola, V., Berdyugin, A., & Berdyugina, S. 2014, in Proc SPIE, 9147, 8
Pogorelov, N. V., Heerikhuisen, J., Mitchell, J. J., Cairns, I. H., & Zank, G. P. 2009, ApJL, 695, L31
Pogorelov, N. V., Heerikhuisen, J., Zank, G. P., et al. 2011, ApJ, 742, 104
Richardson, J. D., & Decker, R. 2014, ApJ, 792, 126
Santos, F. P., Corradi, W., & Reis, W. 2011, ApJ, 728, 104
Santos, F. P., Franco, G. A. P., Roman-Lopes, A., Reis, W., & Román-Zúñiga, C. G. 2014, ApJ, 783, 1
Schwadron, N. A., Allegrini, F., Bzowski, M., et al. 2011, ApJ, 731, 56
Schwadron, N. A., Bzowski, M., Crew, G. B., et al. 2009, Sci, 326, 966
Schwadron, N. A., & McComas, D. J. 2013, ApJ, 764, 92
Schwadron, N. A., Moebius, E., Fuselier, S. A., et al. 2014, ApJS, 215, 13
Serkowski, K., Mathewson, D. S., & Ford, V. L. 1975, ApJ, 196, 261
Slavin, J. D., & Frisch, P. C. 2008, A&A, 491, 53
Slavin, J. D., Frisch, P. C., Müller, H.-R., et al. 2012, ApJ, 760, 46
Spangler, S. R., Savage, A. H., & Redfield, S. 2011, in AIP Conf. Ser. 1366, Ion-Neutral Collisions in the Interstellar Medium: Wave Damping and Elimination of Collisionless Processes, ed. V. Florinski et al. (Melville, NY: AIP), 97
Sterken, V. J., Altobelli, N., Kempf, S., et al. 2012, A&A, 538, A102
Westphal, A. J., & the Stardust Team 2014, Sci, 345, 786 791
Witte, M. 2004, A&A, 426, 835
Wood, B. E., Linsky, J. L., & Zank, G. P. 2000, ApJ, 537, 304
Wood, B. E., Mueller, H.-R., & Witte, M. 2015, ApJ, 801, 62
Zank, G. P., Heerikhuisen, J., Wood, B. E., et al. 2013, ApJ, 763, 20